Materials Science and Engineering B 274 (2021) 115489

Contents lists available at ScienceDirect

Materials Science & Engineering B

journal homepage: www.elsevier.com/locate/mseb

Theoretical studies of energy states of CdSe/ZnS/CdSe and ZnS/CdSe/ZnS quantum dots with an impurity

Abdolali Rabanian [a], Mina Neghabi [a,*], Mehdi Zadsar [a], Mostafa Jafari [b]

[a] Department of Physics, Najafabad Branch, Islamic Azad University, Najafabad, Iran
[b] Department of Mathematics, Najafabad Branch, Islamic Azad University, Najafabad, Iran

ARTICLE INFO

Keywords:
Spherical quantum dot
Energy state
Radial probability distributions
Impurity

ABSTRACT

The energy states of an electron in the presence of impurity ion in center of A: CdSe/ZnS/CdSe and B: ZnS/CdSe/ZnS quantum dots were investigated by the numerical method in the framework of the effective mass approximation. The electronic properties of A and B quantum dots including the binding energy and the radial probability distribution have been calculated as a function of core radius while the outer radius of quantum dots was fixed. It was expected that the arrangement of materials with different energy gaps in the two structures would affect the electronic properties. The numerical results have presented that the geometry of these two quantum dots as well as the effect of the quantum confinement which occurs mainly in the core of structure A and in the shell of structure B, has a significant effect on the electronic properties of quantum dots.

1. Introduction

In recent years, with the improvement of nanotechnology, quantum dots (QDs) are widely used in a variety of electronic devices and applications such as quantum-dots light-emitting diodes [1–3], quantum dot solar cells [4–6], quantum dot lasers [7–9], single-electron transistors [10–12], quantum computing [13–15], single-photon sources [16–18], Second-Harmonic Generation [19–21] and medical imaging [22–24]. It is obvious that the determination of the physical properties of the quantum dots is also necessary due to the widespread use in these various electronic device applications. Because of the great importance of quantum dots as a class of quantum confined structures with excellent optical and electronic properties, several theoretical studies were performed to better understand the electronic structure and the photo physical processes, which occur in these structures. These studies have covered research in the QDs field and many have focused on various aspects of the effect of the QD size [25], the applied potential [26], the impurity [27–29] and the external electromagnetic fields [30] on discrete energy states of an electron.

Many studies about energy states have been studied and proposed. Boze et al., have calculated the energy levels of an electron confined in the spherical GaAs/AlxGa$_{1-x}$As/AlAs quantum dot with the impurity located at the center of the quantum dot [31]. They also have reported the binding energy and the radial probability distribution function of an electron in the 1s, 2s and 2d states for this QD. This study has established that shell thickness ($Al_xGa_{1-x}As$ layer) in the spherical dot dramatically affects the characteristics of the binding energy and radial probability density. Aydin et al., have investigated the electronic properties of a double electron in the CdSe/ZnS/CdSe/ZnS quantum dot for cases with and without an on-center donor impurity [32]. They have examined the binding energies of negatively charged donor impurity (D^-) for different core radii, shell thicknesses, and well widths by solving the Poisson-Schrodinger equations in the frame of the single band effective mass approximation and Hartree treatment. Kasapoglu et al., have investigated the binding energies of the s-symmetric ground and first excited shallow donor impurity states in "12–6" tuned GaAs/GaAlAs double quantum well as a function of the size of the structure, the impurity position and the electric and magnetic field intensities [33]. The obtained results indicate that the electronic properties of this structure well can be adjustable by an appropriate choice of the sample geometry and applied external fields. Rahou et al., have described the electronic features of InSb spherical quantum dots by a pseudopotential approach as a function of their radius [34].

Single semiconductor QDs such as CdSe and ZnS have been extensively considered and used for different electronic and biological device applications [35]. However, Reports show that applications of these single material QDs are limited by the stability and low quantum performance as a result of surface defects which provide nonradiative

* Corresponding author.
E-mail address: neghabi@iaun.ac.ir (M. Neghabi).

https://doi.org/10.1016/j.mseb.2021.115489
Received 27 October 2020; Received in revised form 20 July 2021; Accepted 1 October 2021

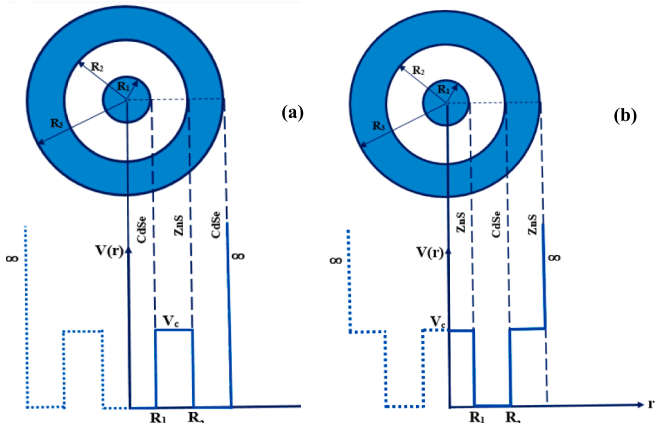

Fig. 1. Schematic illustration of spherical core/shell/shell quantum dot (a) (CdSe/ZnS/CdSe) and (b) (ZnS/CdSe/ZnS) and their potential profile. The radii of core, shell1 and shell2 are R_1, R_2 and R_3, respectively.

Table 1
Structural parameters, effective masses and the confinement potential for both of A and B quantum dots.

Structures	Radius	Effective Massm_i^*	Spherically Symmetric Potential $V_0(r)$
A: CdSe/ZnS/ CdSe	$r \le R_1$	$m_1^* = m_{CdSe}^*$	0
	$R_1 < r \le R_2$	$m_2^* = m_{ZnS}^*$	V_c
	$r \ge R2$	$m_3^* = m_{CdSe}^*$	∞
B: ZnS/CdSe/ ZnS	$r \le R_1$	$m_1^* = m_{ZnS}^*$	V_c
	$R_1 < r \le R_2$	$m_2^* = m_{CdSe}^*$	0
	$r \ge R2$	$m_3^* = m_{ZnS}^*$	∞

processes due to trapping the charge carriers [36]. To avoid of these defects, core–shell type-I QDs such as CdSe/ZnS have been introduced where high band gap material is used as shell to firmly confine the excitons. The significance of growing a shell over the surface of core QDs is making the QDs less sensitive to environmental changes and photo-oxidation and another advantage is the enhancement of quantum yield by elimination of nonradiative trap-related charge-carrier recombination in surface. Despite these features, the inhomogeneous broadening in the optical spectra is often difficult to control in type-I QDs. It is established that line narrowing in the optical spectra is an important issue for optoelectronics device applications. On the other hand, inverse type-I QDs such as ZnS/CdSe where wide band gap core is enclosed in the narrow band gap shell can act as a color filter, which results in a narrowing of the optical spectra. However, the luminescence quantum yield of inverse type-1 QDs is poor, compared to type-1 QDs, might be due to charge transfer quenching in surface states which limits their use in high-performance optoelectronic and luminescent biological devices.

In yet another technique, core–shell-shell structures can offer new outlook for increasing quantum yield and tuning the optical properties in QDs by regulating the thickness of sandwiched and outer shells. For example, CdSe/ZnS/CdSe and ZnS/CdSe/ZnS QDs illustrate narrow mono-color [37] and multi-color emission with high quantum efficiency [38] by coupling and decoupling between charge carriers of their core and outer shells. Therefore, investigating energy states of these QDs and determining their electronic properties have a fundamental importance from theoretical and application point of view.

In this paper we study two core/shell/shell spherical quantum dot heterostructures of A: CdSe/ZnS/CdSe and B: ZnS/CdSe/ZnS for cases with and without a center impurity. In the structure of A, the band gap of the core is smaller than the band gap of the shell. While, the core

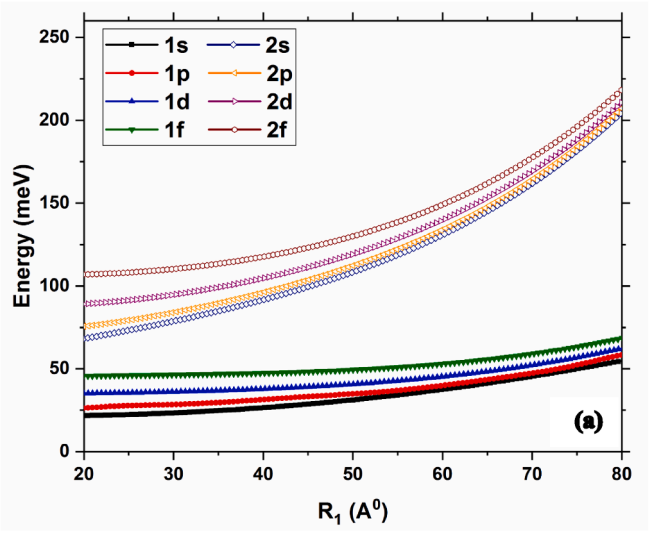

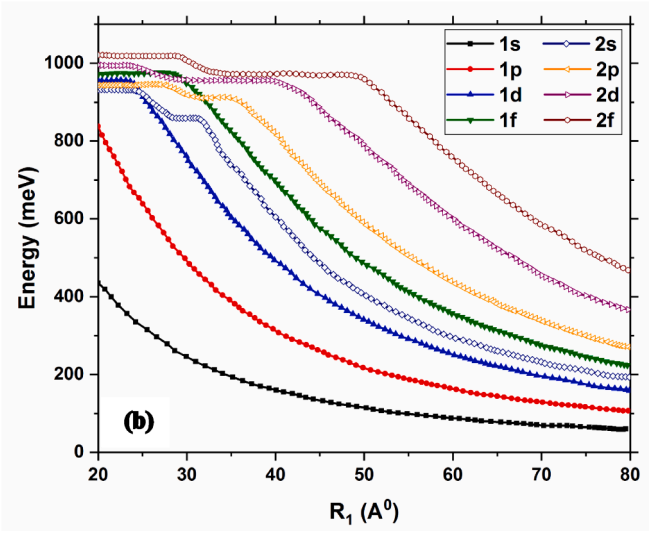

Fig. 2. Energy levels of (a) the spherical CdSe/ZnS/CdSe quantum dot and (b) the spherical ZnS/CdSe/ZnS quantum dot with the impurity as functions of the core radius for constant R_2.

encapsulated with a shell that has a larger band gap in the structure of B. We compare the energy levels of these two structures and report the detailed calculation of their binding energies and probability densities. Since the ZnS band gap as core (shell) is much larger than that of CdSe as shell (core), it is expected that electronics properties of these two structures be different.

2. Theory and calculation

We consider two spherical core/shell/shell quantum dots in the structures of A: CdSe/ZnS/CdSe and B: ZnS/CdSe/ZnS. We assumed that the structure of A is composed of CdSe core and ZnS and CdSe shells. While the core of the structure of B is ZnS that is enveloped by the CdSe and ZnS shells. However, both the A and B structures have core with inner radius R_1 and shells with R_2 and R_3 radii, as showed in Fig. 1. It is seen that these structures are defined as the one-step infinity quantum dots.

We use the numerical method in the framework of the effective mass approximation to model the A and B QDs, which are assumed to have perfect spherical symmetry.

The Hamiltonian of an electron confined in each of A and B QDs in the presence of on-center hydrogenic impurity can be described as:

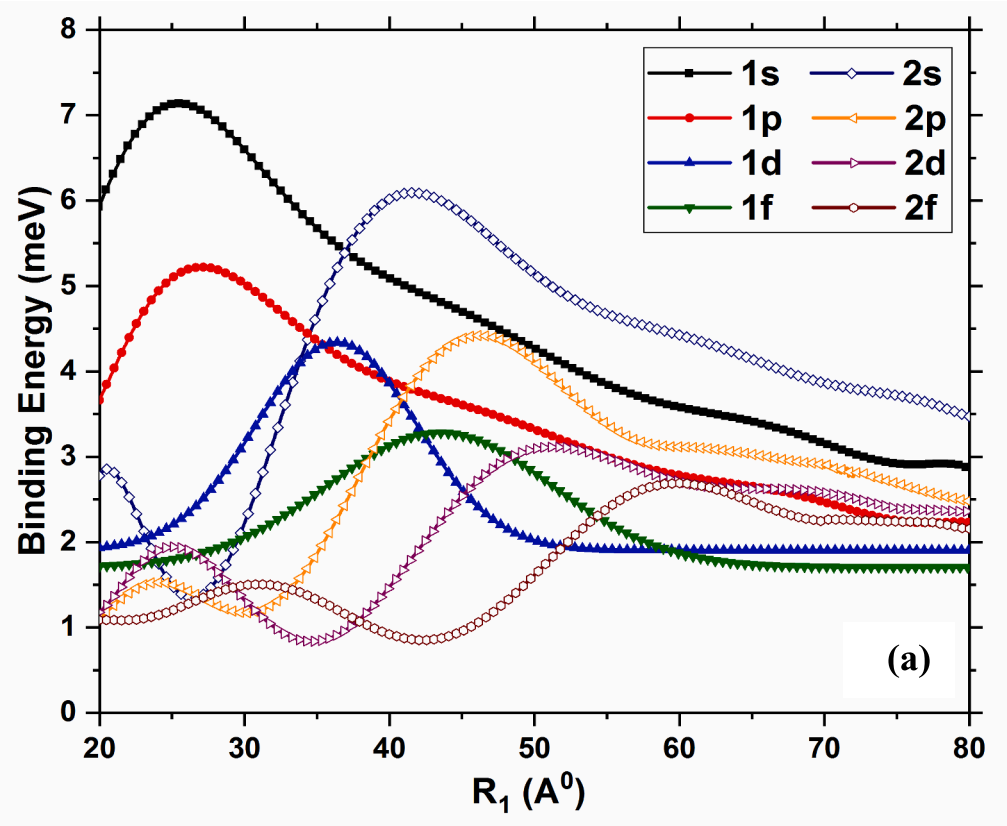

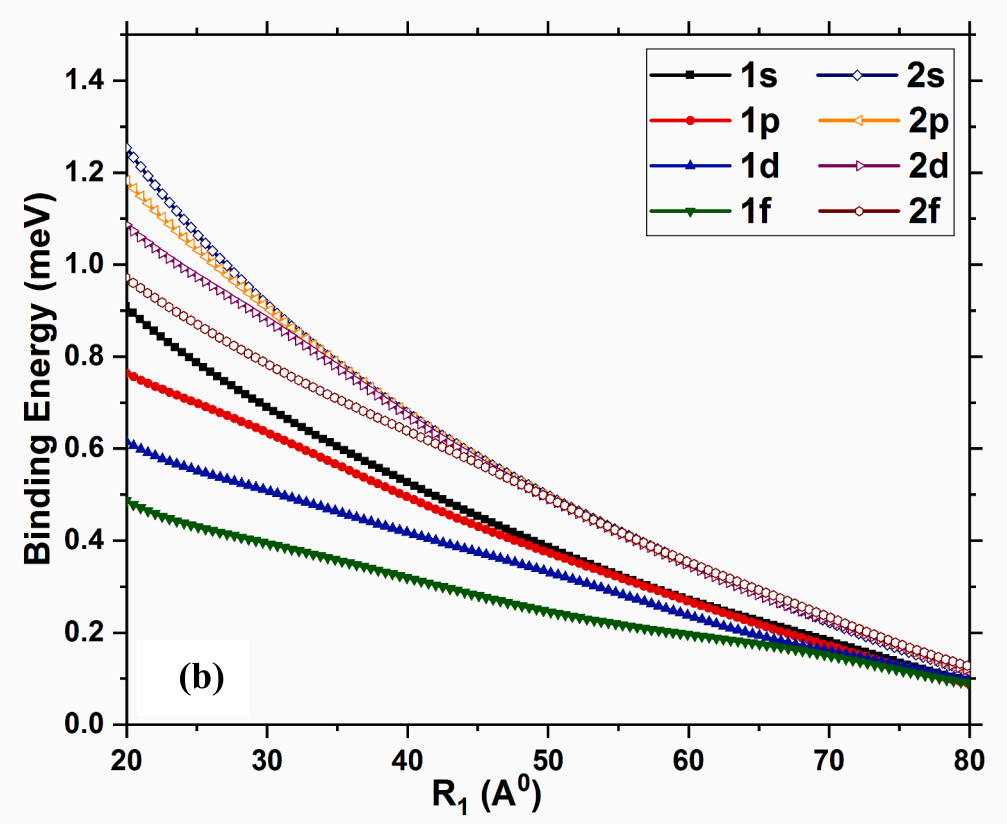

Fig. 3. Variation of binding energies of (a) the spherical CdSe/ZnS/CdSe quantum dot and (b) the spherical ZnS/CdSe/ZnS quantum dot as functions of the core radius for the various energy and constant R_2.

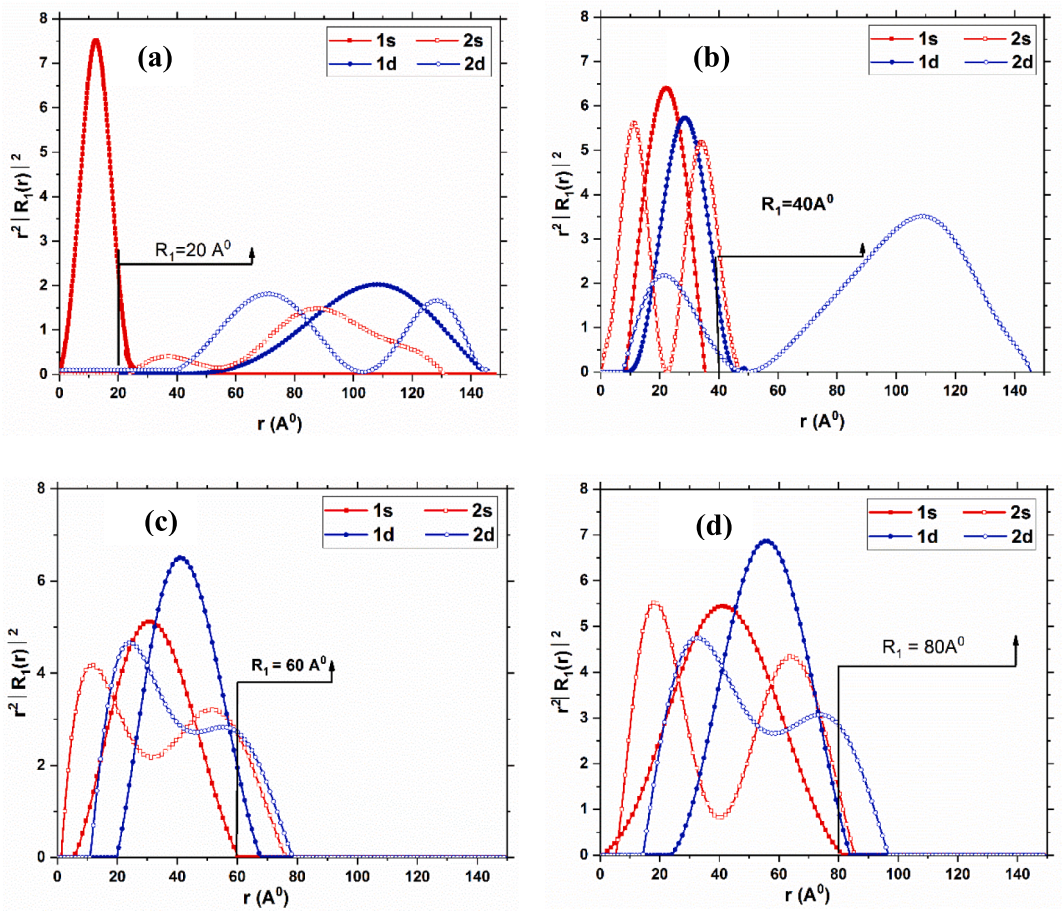

Fig. 4. Probability distribution of 1s, 2s, 1d and 2d states in the spherical A-QD (CdSe/ZnS/CdSe) for four different values of R_1 radius.

$$H = H_0 + U(r) \tag{1}$$

where H_0 and U(r) denote the Hamiltonian of an electron and the Coulomb interaction of the electron with the impurity in a nonuniform dielectric medium, respectively. The expression of H_0 is written as:

$$H_0 = -\frac{\hbar^2}{2m_i^*}\nabla^2 + V_0(r) \tag{2}$$

where the first term is the Hermitian kinetic energy operator for an effective mass m_i^* of a localized electron in the i^{th} region, and V_0 (r) is the confinement potential with spherically symmetry. These terms are listed in Table 1 for both of A and B quantum dots.

It is assumed that the potential in the core and shell material as the zero reference energy for A and B QDs, respectively. Since the band gap of ZnS is wider than that of CdSe for both of QDs, thus the value of V_c as the potential energy jump at the boundary of the core and the shell is larger than zero ($V_c > 0$). In Eq. (1), the electron-impurity interaction is described with the term U(r) as the potential energy of an electron in both structures. This parameter is achieved by solving the Poisson equation in the considered spherical quantum dots, and using the boundary conditions [39].

$$\mathrm{U(r)} = \begin{cases} \dfrac{-e^2}{\varepsilon_1 r} + \dfrac{e^2}{\varepsilon_1 R_1}\left(1 - \dfrac{\varepsilon_1}{\varepsilon_2}\right) + \dfrac{e^2}{\varepsilon_2 R_2}\left(1 - \dfrac{\varepsilon_2}{\varepsilon_3}\right), r \le R_1 \\ \dfrac{-e^2}{\varepsilon_2 r} + \dfrac{e^2}{\varepsilon_2 R_2}\left(1 - \dfrac{\varepsilon_2}{\varepsilon_3}\right), R_1 < r < R_2 \\ \dfrac{-e^2}{\varepsilon_3 r}, r \ge R_2 \end{cases} \tag{3}$$

here ε_1, ε_2 and ε_3 are the dielectric constants of the core, the first shell and the last shell respectively, for the both of QDs.

The Schrödinger equation is used to find the eigenfunctions ($\Psi_{n,l,m}$) of the Hamiltonian in Eq. (1) and their corresponding energies E, so that it can be written as:

$$\left(-\frac{\hbar^2}{2m_i^*}\nabla^2 + V(r) + U(r)\right)\Psi_{n,l,m} = \mathrm{E}\Psi_{n,l,m} \tag{4}$$

here, the subscript n is the principal quantum number and the subscripts l and m are the angular momentum quantum numbers with and ($l < m < +l$).

Due to spherical symmetry of QDs, the eigenfunction may be given by $\Psi_{n,l,m} = R_{n,l}(r)\, Y_{l,m}(\theta,\varphi)$ where $R_{n,l}$ (r) is the radial part and $Y_{l,m}(\theta,\varphi)$ is the spherical harmonics of the wave function. The energy states and wave function are obtained from the solution of the radial Schrödinger equation, written as:

$$\left\{-\frac{\hbar^2}{2m_i^*}\left[\frac{d^2}{dr^2} + \frac{2}{r}\frac{d}{dr} - \frac{l(l+1)}{r^2}\right] + V(r) + U(r)\right\}\mathrm{R}_{n,l} = E_{n,l}\mathrm{R}_{n,l} \tag{5}$$

In order to achieve reasonable expressions of the eigenenergies and their corresponding wave functions, the continuity conditions at all boundaries of the studied A and B QDs must be satisfied as follows:

$$\begin{cases} \mathrm{R}_{n,l}(r_i) = R_{n,l}(r_{i+1})\big|_{r=r_i} \\ \dfrac{1}{m_i^*}\dfrac{d\mathrm{R}_{n,l}(r_i)}{dr} = \dfrac{1}{m_{i+1}^*}\dfrac{d\mathrm{R}_{n,l}(r_{i+1})}{dr}\Big|_{r=r_i} \end{cases} \tag{6}$$

The solution procedure of Eq. (5) is realized on the basis of numerical calculations. In order to exploit the accurate solution of the numerical

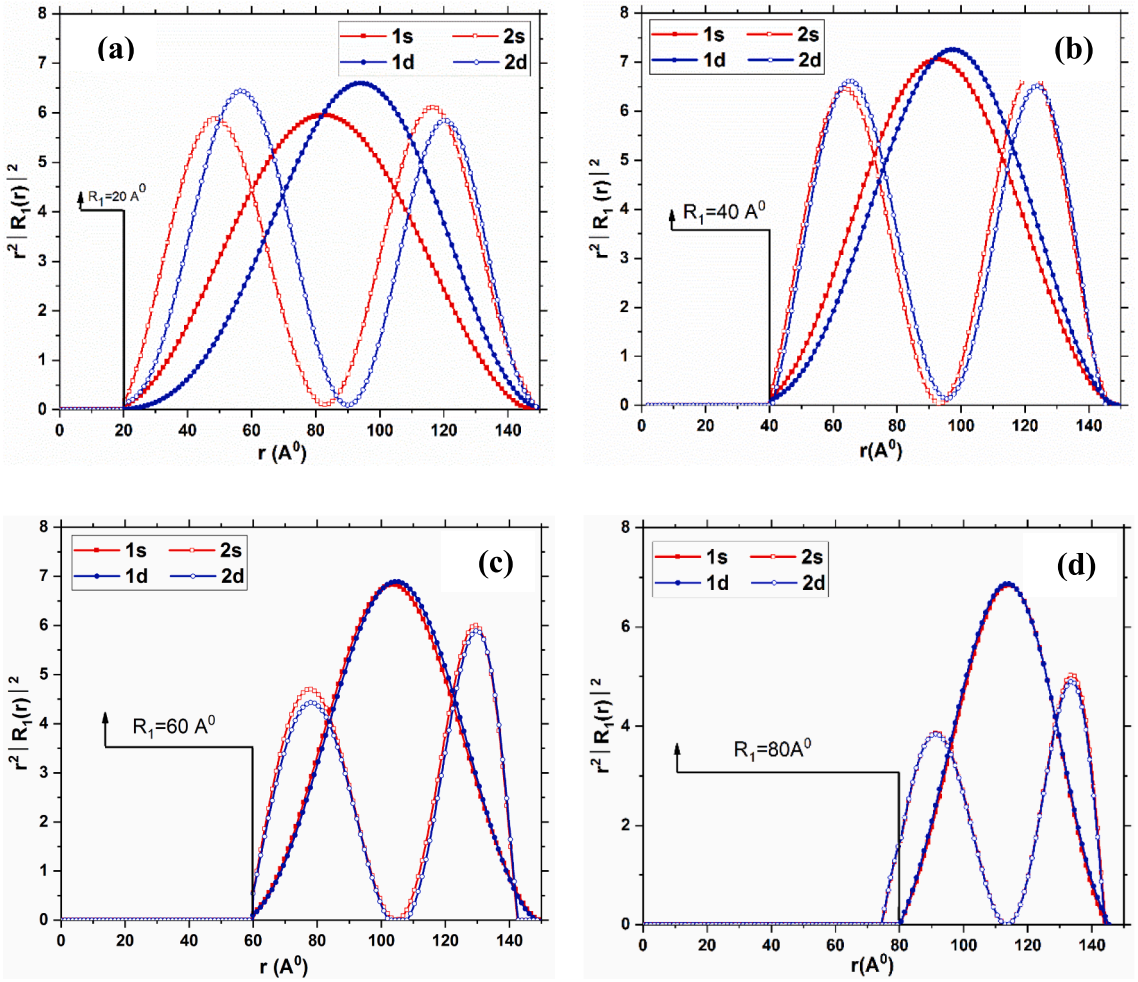

Fig. 5. Probability distribution of 1s, 2s, 1d and 2d states in the spherical B-QD (ZnS/CdSe/ZnS) for four different values of R_1 radius.

method, the step-by-step integration process is checked by error accuracy.

3. Numerical results

In our calculations, the following parameters are use: $m^*_{CdSe} = 0.13m_0$, $m^*_{ZnS} = 0.28m_0$, $E_{gCdSe} = 1.84eV$, $E_{gZnS} = 3.54eV$, $\varepsilon_{CdSe} = 9.56eV$, $\varepsilon_{ZnS} = 3.54eV$ and $V_c = 900eV$ [39,40].

Considering the impurity at center of each of A and B spherical QDs, the single electron eigenenergies has been calculated for the s, p, d and f states. We have explored the electronic properties of the spherical CdSe/ZnS/CdSe and ZnS/CdSe/ZnS quantum dots in the case of the last shell radius R_2 depicted in Fig. 1 is constant while the radius of the core sphere is varied.

Remarkably, the energy levels of the electron for A and B QDs in this case are given as a function of the core radius R_1 increases to 80 A° , where $R_2 = 150$ A° is a fixed parameter in Fig. 2a and b. It is found that in the case of A QD, for the first (1s, 1p, 1d and 1f) state energies, the eigenenergies are completely reduced as the size of the core increased for both 1s and 1p, indicating that electron confined in the core and the effect of quantum confinement befalls on the electron. While for 1d and 1f states, there is a steady trend first and then decreases. In fact, the electron confinement has not occurred for the small core radii and energies are almost constant up to $R_1 = 25$ A^0 and $R_1 = 30$ A^0 for 1d and 1f states, respectively. But when the core radius (R_1) increases, the electron confinement is relieved. On the other hand, the second (2s, 2p, 2d and 2f) state energies have a second flattening which indicates that the probability distribution will have two peaks. When the energies are on the second flattening, the second peak is outside the core, and this is because the size of the core is still insufficient to confine the second peak. However, it can be seen that this second peak penetrates into the core as the energy decreases uniformly.

Fig. 2b shows that there is a sharp difference between the trends of energy changes in terms of R_1 for B-QD compared to A-QD. For B-QD, it is obvious that the eigenenergies have an increasing trend for all the first (1s-1f) and second (2s-2f) levels. However, the energy of the first states essentially are lower than those of the second states. The obvious reason for this increasing is that in the B-QD, the electron confined within the inner shell (CdSe) and can't penetrate into the inner dot duo to potential barrier applied by ZnS core layer.

We determined the variation of the binding energies with the increasing inner dot sphere radius for A and B QDs, exhibited in Fig. 3a and b, respectively. In the A-QD, the binding energies of the first (1s-1f) levels appear with a different behavior compared to those for second (2s-2f) levels. In fact, the binding energy of the first (1s-1f) levels contain a maximum which follows by the smoothly decreasing trend while there are two maxima for the binding energy of the second (2s-2f) states in the range of R_1. For first (1s-1f) states, it can be inferred that the decrease in the binding energy is attributed to the weakening Coulomb interaction between the impurity located at r = 0 and electron. This result can be confirmed by examining the probability distribution function in Fig. 4a-d where the 1s, 1d, 2s and 2d states are chosen as the representatives.

As can be seen from Fig. 4a-d, the probability distributions of the first states (1s and 1d) include a peak. According to Fig. 4a, for 1s state, the intensity of peak with a maximum of around $R_1 = 15\ A^0$ is higher than other first states. This indicates that the electron is strongly confined in the core layer and consequently delivers the maximum binding energy. After that, the intensity of the probability distribution peak as the binding energy decreases with the increasing radius of the inner core as in Fig. 4b-d and 3. On the other hand, for the other first state (1d), the probability distribution initially has a maximum inside the shell layer, which corresponds to the maximum binding energy of this state and then the binding energy decreases as the distance between the electron and the impurity increases with the increasing radius of the core and consequently the probability distribution penetrates into the inner core as in Fig. 4b-d.

For the second states (2s and 2d), the probability distribution has two peaks corresponding to the maxima of binding energy as in Fig. 4a-d. For the 2s state, the first maximum is near the core and the other is far from the core for $R = 20\ A^0$. The electron–impurity interaction is not yet strong and the second peak of the probability distribution is within the shell which can be observed in Fig. 4a. As the radius increases to $R = 40\ A^0$, the electron becomes strongly confined in the core and the second peak penetrates into the inner core, and this trend continues as the radius of core increases further as presented in Fig. 4b and d. The other second state (2d) behave as 2s state, except that the maximum binding energy is about $R1 = 50\ A^0$, and the second peak of the probability distribution penetrates into the inner core in $R_1 = 60\ A^0$.

Finally, we discuss the binding energy and the probability distribution of B-QD which is described above as ZnS and CdSe were introduced as the core and first shell, respectively. Fig. 3 shows the variation in binding energy of B-QD for different thickness of core layer (R_1). It can be seen that the binding energy of B-QD decreases when R_1 radius varies from 20 A^0 to 80 A^0 and this is while the energies of the second states (2s-2f) fall in higher binding energies than the first states (1s-1f). Since the impurity is located in the center of the core and the ZnS core acts like a potential well, there is always a potential barrier between the electron and the impurity ion. As the diameter of the core increases, the distance between the electron and the impurity increases, and consequently the Coulomb interaction between them weakens, and therefore the binding energy decreases.

Accordingly, when examining the electron probability distribution function in terms of the radius R_1 shown in Fig. 5a-d, it is found that all the peaks of the probability distribution are located in the CdSe shell and approach each other as the radius R_1 increases and do not penetrate into the inner core. This result agrees with the behavior of the binding energy of B-QD.

4. Conclusion

We investigated the electronic properties of two quantum dots with structures of A: CdSe/ZnS/CdSe and B: ZnS/CdSe/ZnS by using a numerical modeling. The calculations were performed while the total radius of the quantum dot remained constant and the radius of the core (R_1) increased. It was found that the changes in core layer thickness can affect the radial distribution functions and binding energies of the A and B QDs. For the A-QD, the behavior of the binding energy of the first (1s, 1p, 1d, 1f) states is different from that of second (2s, 2p, 2d, 2f) states, which can be explained based on the effect of quantum confinement and the probability distribution of these states. However, the binding energy of all the first and second states of B-QD decrease with the increase of the core radius. Also, the probability distribution of B-QD indicates that all the peaks are located in the CdSe shell layer and do not penetrate into the core. Numerical modeling results established that the binding energy and the probability distribution are the important factors to design and fabricate quantum dots with optimal electronic properties in laboratory processes.

Declaration of Competing Interest

The authors declare that they have no known competing financial interests or personal relationships that could have appeared to influence the work reported in this paper.

Acknowledgment

Authors are thankful to the Islamic Azad University, Najafabad Branch Research Council for the partial support of this research.

Data availability.

The raw/processed data required to reproduce these findings cannot be shared at this time as the data also forms part of an ongoing study.

References

[1] X. Jin, et al., Thick-shell CdZnSe/ZnSe/ZnS quantum dots for bright white light-emitting diodes, J. Lumin. (2020), 117670.
[2] B. Deng, et al., Low temperature synthesis of highly bright green emission CuInS2/ZnS quantum dots and its application in light-emitting diodes, J. Alloy. Compd. (2020), 155400.
[3] Y. Ye, et al., Efficient multi-shell CuInS2/ZnS/ZnS quantum-dots based light-emitting diodes: Time-controlled synthesis of quantum-dots and carrier balance effects of PEI, Opt. Mater. 106 (2020), 109926.
[4] A. Ganguly, S. Nath, Mn-doped CdS quantum dots as sensitizers in solar cells, Mater. Sci. Eng., B 255 (2020), 114532.
[5] A. Wang, et al., *Advances in perovskite quantum-dot solar cells.* Journal of Energy, Chemistry (2020).
[6] H. Latif, et al., A novel, PbS quantum dot-Sensitized solar cell structure with TiO2-fMWCNTS nano-composite filled meso-porous anatase TiO2 photoanode, Sol. Energy 204 (2020) 617–623.
[7] N. Radzi, et al., Q-switched fiber laser based on CdS quantum dots as a saturable absorber, Results Phys. 16 (2020), 103123.
[8] M. Barseghyan, et al., Control of electronic and optical properties of a laser dressed double quantum dot molecule by lateral electric field. Phys. E: Low-dimension. Syst. Nanostruct. 126: 114362.
[9] Yousefvand, H.R., Impact of carrier heating on performance of quantum-dot semiconductor lasers: Theoretical study and circuit-level modeling. Optics Communications. 478: p. 126395.
[10] A. Moulhim, B. Tripathi, M. Kumar, Investigating the effect of quantized confining energy on the quantum coulomb blockade phenomena in single-electron transistor, Solid State Commun. (2020), 114078.
[11] H. Ali, et al., Single-electron pumping in a ZnO single-nanobelt quantum dot transistor, Sci. China Phys. Mech. Astron. 63 (6) (2020), 267811.
[12] V. Khademhosseini, et al., Current analysis of single electron transistor based on graphene double quantum dots, ECS J. Solid State Sci. Technol. 9 (2) (2020), 021003.
[13] B. Hensen, et al., A silicon quantum-dot-coupled nuclear spin qubit, Nat. Nanotechnol. 15 (1) (2020) 13–17.
[14] T. Kodera, Silicon quantum dot devices for spin-based quantum computing. 2020 IEEE Silicon Nanoelectronics Workshop (SNW), IEEE, 2020.
[15] L. Ricco, et al., Interaction induced hybridization of Majorana zero modes in a coupled quantum-dot–superconducting-nanowire hybrid system, Phys. Rev. B 102 (16) (2020), 165104.
[16] H. Ollivier, et al., Reproducibility of high-performance quantum dot single-photon sources, ACS Photon. 7 (4) (2020) 1050–1059.
[17] A. Baride, et al., One-and two-photon electron-transfer induced uncaging of coumarin from cinnamate-capped CdSe quantum dots, J. Lumin. (2020), 117112.
[18] A. Kotb, C. Guo, All-optical NOR and XNOR logic gates at 2 Tb/s based on two-photon absorption in quantum-dot semiconductor optical amplifiers, Opt. Quant. Electron. 52 (1) (2020) 30.
[19] D. Makhlouf, et al., Modeling of the second harmonic generation in a lens-shaped InAs/GaAs quantum core/shell dot under temperature, pressure and applied electric field effects, Results Phys. 16 (2020), 102961.
[20] S. Evangelou, Comment on "Tunneling effect on second-harmonic generation in quantum dot molecule, Superlattices and Microstructures 91 (2016) 358-364", Superlatt. Microstruct. (2020) 106708.
[21] S. Arif, et al., Analyzing role of relaxation time on second harmonic generation and optical dielectric function of impurity doped quantum dots under the aegis of noise, Phys. B (2020), 412166.
[22] H.M. Kashani, et al., Bottom-up and green-synthesis route of amino functionalized graphene quantum dot as a novel biocompatible and label-free fluorescence probe for in vitro cellular imaging of human ACHN cell lines, Mater. Sci. Eng., B 251 (2019), 114452.
[23] M. Rana, et al., Glutathione capped core/shell CdSeS/ZnS quantum dots as a medical imaging tool for cancer cells, Inorg. Chem. Commun. 112 (2020), 107723.
[24] H. Liang, et al., Carbon quantum Dot@ Silver nanocomposite–based fluorescent imaging of intracellular superoxide anion, Microchim. Acta 187 (9) (2020) 1–9.
[25] J.A. Vinasco, et al., Effects of geometry on the electronic properties of semiconductor elliptical quantum rings, Sci. Rep. 8 (1) (2018) 13299.

[26] R. Khordad, B. Mirhosseini, M.M. Mirhosseini, Thermodynamic properties of a GaAs quantum dot with an effective-parabolic potential: theory and simulation, J. Low Temp. Phys. 197 (1) (2019) 95–110.
[27] O. Akankan, et al., The effects of geometrical shape and impurity position on the self-polarization of a donor impurity in an infinite GaAs/AlAs tetragonal quantum dot, Indian J. Phys. (2020).
[28] L. Stevanović, et al., Theoretical investigation of the transient regime of electromagnetically induced transparency in spherical quantum dot with on-center hydrogen impurity, Opt. Quant. Electron. 52 (3) (2020) 1–10.
[29] O. Akankan, et al., The effects of geometrical shape and impurity position on the self-polarization of a donor impurity in an infinite GaAs/AlAs tetragonal quantum dot, Indian J. Phys. (2020) 1–4.
[30] J.A. Osorio, et al., Pyramidal core-shell quantum dot under applied electric and magnetic fields, Sci. Rep. 10 (1) (2020) 8961.
[31] F.K. Boz, et al., Energy levels of GaAs/AlxGa1-xAs/AlAs spherical quantum dot with an impurity, Appl. Surf. Sci. 387 (2016) 76–81.
[32] R. Aydin, M. Sahin, The electronic properties of a two-electron multi-shell quantum dot-quantum well heterostructure, J. Appl. Phys. 114 (4) (2013), 043706.
[33] E. Kasapoglu, et al., Binding energy and optical absorption of donor impurity states in "12-6" tuned GaAs/GaAlAs double quantum well under the external fields, Phys. B 554 (2019) 72–78.
[34] D. Rahou, et al., Electronic and optical properties of InSb quantum dots from pseudopotential calculation, Chin. J. Phys. (2020).
[35] S.O. Hinterding, et al., Single trap states in single CdSe nanoplatelets, ACS Nano 15 (4) (2021) 7216–7225.
[36] K.A. Svit, et al., Crystal structure and predominant defects in CdS quantum dots fabricated by the Langmuir-blodgett method, Langmuir 37 (18) (2021) 5651–5658.
[37] S. Nizamoglu, H.V. Demir, Onion-like (CdSe) ZnS/CdSe/ZnS quantum-dot-quantum-well heteronanocrystals for investigation of multi-color emission, Opt. Express 16 (6) (2008) 3515–3526.
[38] R. Kostić, D. Stojanović, Multi-color emission in quantum-dot–quantum-well semiconductor heteronanocrystals, Act. Phys. Polon. A 116 (2009) 598–602.
[39] D. Stojanović, R. Kostić, Hydrogenic impurity states in the spherical CdSe/ZnS/CdSe nanoheterostructure, Opt. Quant. Electron. 48 (4) (2016) 226.
[40] N. Zeiri, et al., Quadratic optical effects in ZnS/CdS/ZnS quantum dot-quantum well, Results Phys. 14 (2019), 102513.